Sensing and Imaging (2023) 24:10
https://doi.org/10.1007/s11220-023-00413-w

RESEARCH

# A Review of Quartz Crystal Microbalance for Chemical and Biological Sensing Applications

**Nadyah Alanazi[1] · Maram Almutairi[1] · Abdullah N. Alodhayb[1,2]**

Received: 19 June 2022 / Revised: 21 January 2023 / Accepted: 26 January 2023 /
Published online: 4 March 2023


## Abstract

Humans are fundamentally interested in monitoring and understanding interactions that occur in and around our bodies. Biological interactions within the body determine our physical condition and can be used to improve medical treatments and develop new drugs. Daily life involves contact with numerous chemicals, ranging from household elements, naturally occurring scents from common plants and animals, and industrial agents. Many chemicals cause adverse health and environmental effects and require regulation to prevent pollution. Chemical detection is critically important for food and environmental quality control efforts, medical diagnostics, and detection of explosives. Thus, sensitive devices are needed for detecting and discriminating chemical and biological samples. Compared to other sensing devices, the Quartz Crystal Microbalance (QCM) is well-established and has been considered and sufficiently sensitive for detecting molecules, chemicals, polymers, and biological assemblies. Due to its simplicity and low cost, the QCM sensor has potential applications in analytical chemistry, surface chemistry, biochemistry, environmental science, and other disciplines. QCM detection measures resonate frequency changes generated by the quartz crystal sensor when covered with a thin film or liquid. The quartz crystal is sandwiched between two metal (typically gold) electrodes. Functionalizing the electrode's surface further enhances frequency change detection through to interactions between the sensor and the targeted material. These sensors are sensitive to high frequencies and can recognize ultrasmall masses. This review will cover advancements in QCM sensor technologies, highlighting in-sensor and real-time analysis. QCM-based sensor function is dictated by the coating material. We present various high-sensitivity coating techniques that use this novel sensor design. Then, we briefly review available measurement parameters and technological interventions that will inform future QCM research. Lastly, we examine QCM's theory and application to enhance our understanding of relevant electrical components and concepts.

Extended author information available on the last page of the article

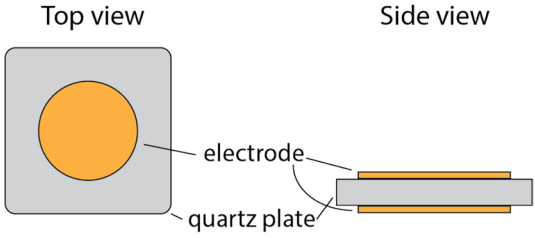


**Fig. 1** A schematic showing the top and side view of a basic QCM structure. Reproduced with permission from Ref. [10]

**Keywords** Quartz crystal microbalance · Crystal oscillators · Chemical sensors · Biosensors

## 1 Introduction

Mass and weight measurements are central to human curiosity and have been from the beginning of time. The earliest method for measuring mass involved balancing two weights at opposite ends of a stick suspended by its center. While this method is still widely used, more sophisticated, indirect techniques have been developed over time; for example, measurements of spring expansion after mass loading. Such techniques are accurate, precise, and capable of measuring even small masses. Others have used cyclotrons or resonators to measure mass. Resonators, in particular, have improved the mass measurement accuracy, precision, and resolution [1]. Resonators are based on bulk acoustic waves (BAWs) and are versatile and robust methods for measuring mass. Unfortunately, these methods feature a minimum mass that can be measured. However, *miniaturized* BAW resonators can create high-sensitivity gravimetric sensors, making measurement of even a few atoms or molecules possible in laboratory conditions.

Quartz Crystal Microbalance (QCM) is a notable BAW resonator-based mass sensor [2]. The piezoelectric effect, discovered in 1880 by French physicists Jacques and Pierre Curie [3], improved our understanding of the electromechanical interactions that exist between crystalline materials' electrical and mechanical states without inversion symmetry [4]. After that, scientists began to explore electromechanical areas and their relationships. In 1959, a research team led by Sauerbrey, a German physicist, examined the relationship between mass absorption on a quartz surface and its frequency offset during the gas phase. Their findings established the foundation for QCM research in various scientific disciplines [5].

The QCM is an acoustic wave sensor [6, 7] that gained popularity due to its extreme sensitivity to mass changes in the nano-scale regime per unit area [6–9]. A typical QCM, as shown in Fig. 1, comprises an AT-cut quartz resonator disc sandwiched between key-hole-shaped metal electrodes [10] and with a central sensor [10]. The AT-cut quartz is a thin wafer sliced out of a rod at a 35° angle relative to the x-axis. The crystal offers low-temperature and high-frequency stability [11, 12, 13]. Later, King et al. used a QCM sensor for chemical analysis through a series of gas detection experiments that included the QCM sensor was put into practice;

these experiments were previously reviewed [11–13]. Recently, Kanazawa et al. [14] devised a theoretical model to explain the correlation between frequency response and QCM sensor parameters and liquid. Bruckenstein and Shay [15] and colleagues authored a similar equation, subsequently verified by experiments.

In brief, piezoelectric sensors directly contact testing solutions to acquire real-time data on QCM sensor surface reactions. After application of an alternating electric field to the quartz crystal, the crystal will resonate at the applied field's frequency secondary to the Converse Piezoelectric Effect. The Direct Piezoelectric Effect generates an electric field inside a crystal following application of mechanical strain. The Converse Piezoelectric Effect, as used in quartz oscillators, applies alternating electric fields to crystals to produce mechanical vibrations.

Piezoelectric sensor research comprises active and passive subdistinctions [16, 17]. The active or "oscillating" method requires connecting the sensor to an oscillator amplifier circuit to provide positive feedback. The piezoelectric crystal's own vibrates can be measured using a frequency counter. The passive method requires the piezoelectric crystal be externally connected to the instrument's measuring port, such as an impedance or spectrum analyzer, Sine waves of different frequencies are created on two of the piezoelectric crystal's sides; the crystal's output signals are subsequently recorded. By comparing input and output signals, the object could acquire crystal-like impedance, admittance, phase, et cetera. At present, most piezoelectric sensors are positioned to directly contact the testing solution and acquire real-time data on the QCM sensor's surface reactions. Additionally, piezoelectric sensor use is mainly based on the mass-sensitive properties of piezoelectric material; the sensor's frequency is affected by the mass absorbed on its. Consequently, piezoelectric sensors are sometimes referred to as "mass piezoelectric sensors." All mass piezoelectric sensors use the Sauerbrey equation to measure mass changes (see Eq. 1). The Sauerbrey equation confirms the linearity between incremental mass changes and resonant frequency [5].

$$\Delta f = -\frac{2f_o^2}{\sqrt{E\rho}} \times \frac{\Delta m}{A} \tag{1}$$

where $\Delta f$ is the resonant frequency, E is Young's modulus, $\rho$ is the density, and A is the area.

Equation 1 is only valid for uniform and rigid films with acoustic properties similar to quartz; it also assumes that the density and transverse velocity of the material are the same as quartz. However, some piezoelectric sensors have been applied to nonmass research—including determination of viscosity, density, stress, viscoelasticity, conductivity, dielectric, and surface properties. Schmittl et al. adopted piezoelectric sensors for measuring the liquid phase's electrical and mechanical characteristics [18]. Moreover, the researchers determined the best cutting angle (AT-cut) to improve stability under ambient temperatures. Kanazawa et al. noted that the sensor's absorbed mass and the deposition film's mechanical characteristics affected the frequency response [19]. The researchers established an electric–mechanical model to explain how sensor deposition film features affected the sensor's frequency response. This model could be applied to both steady and transient states.

Piezoelectric material comprises the sensor's core and acoustic wave spread measures can be made. This spread is influenced by the medium's properties, cutting direction, and thickness. Utilizing different transducers could stimulate different kinds of acoustic waves. The various biosensor acoustic waves include the BAW, surface acoustic wave (SAW) [20, 21], acoustic plate mode (APM) [22, 23], and love wave (LW) [24, 25]. The BAW produced a wide pattern of acoustic waves in piezoelectric sensor applications because of its spread throughout the medium. QCM is a piezoelectric sensor that depends on BAW mode.

The QCM resonance response can be modeled mechanically using the mass-spring-damper system [3, 26, 27]. The mechanical analogy of the resonance response of the QCM is a mass $m$ attached to a spring with spring constant $k$ that is parallel to a damper with a coefficient of friction $\eta$ [1, 12, 13].

The mechanical representation can be converted to an electrical model through the electromechanical coupling factor k [10] using Worth–Van Dyke (BVD), an equivalent circuit [28]. The electrical BVD configuration is typically used to describe QCM without the added mass or liquid loads [20]. In this model, a static capacitance is placed parallel to an LCR series [28]. The LCR branch in the circuit is the motional arm associated with the quartz's shear motion [1, 9, 10, 28]. Static capacitance stands for energy stored between the quartz and electrode surfaces (here, quartz functions as a dielectric) [1, 10], wiring, and crystal holder [1, 10, 28].

Impedance is a complex vector expressed as $Z = R + Xi$, where R is the resistance and X is the reactance. The real part is the dissipated energy, while the imaginary part is the stored energy [10]. For resonance to occur in the BVD circuit, the imaginary part of the impedance must equal zero [1].

This short literature review provides insights into the various QCM measures, along with the underlying principles and relevant technological interventions. We then summarize QCM sensing techniques for biological and chemical samples. QCM is a versatile technology that has been used to detect SARS-CoV-2, the virus responsible for COVID-19. Following our review, we discuss key features of QCM and their value to ongoing scientific efforts to develop low-cost smart sensors.

## 2 Biological Sensors

Biological sensors utilize the direct relationship between mass and frequency found in Sauerbrey's equation [1, 6]. Biosensor analytical devices consist of a receptor that captures targets and a transducer mechanism that produces a signal response [6] when the QCM is paired with a suitable receptor layer to assist with targeted analyte binding.

Biomolecules can alter the viscoelastic properties of the sensor's surface, thereby disrupting the sensor's signal response [1]. Hydrophilic surfaces—either the QCM surface or an adsorbed film—change the sensor's frequency response as liquid becomes entrapped in the sensor's small cavities, increasing the detected mass [1]. Hydrophobic surfaces, on the other hand, do not trap any liquid. This creates an inclusion zone of air or vacuum, leading to energy loss [1].

Pohanka [29] discussed the applications and principles of piezoelectric immunosensors, molecularly imprinted polymers, genetic information biorecognition, and other biosensors. Analytical piezoelectric immunosensor devices use antibodies or antigens as the recognition element. Antibody specificity influences the sensor's overall specificity. These observations led to the use of antigens for diagnosing infectious diseases. Molecularly imprinted polymers (MIPs) are artificial materials that could replace an antibody's or antigen's recognition layer. These artificial elements use a temple in their synthesis process, potentially the same compound as the analyte. Smaller temples are favored over large ones since larger ones could destroy the whole sensor. Materials for MIP construction include sol–gel, chitosan, and dextrin. Genetic information such as DNA or RNA single-strand short strains can serve as a biorecognition layer over the QCM surface. The DNA QCM biosensor is shown in Fig. 2. First, the double-stranded DNA in a sample is denatured (e.g., by heat). Then, a single-stranded DNA hybridizes with an immobilized DNA strand on the QCM surface. Finally, hybridization decreases QCM frequency fluctuations. These biosensors could be used to diagnose genetically determined diseases. A QCM sensor with hybridized gold nanoparticles and a DNA probe could be used to analyze point mutations in the beta-thalassemia gene in codon DC17. Other than that, a combination of quantum dots and magnetic nanoparticles such as iron oxide/gold (magnetic nanoparticles) and CdS quantum dots are covered with a DNA probe. A second probe was a single-stranded DNA. The remaining chain of the analyzed strain of DNA reacts with the unlabeled second probe. The assembly is fixed on the QCM surface by a magnet. The following section discusses two types of QCM sensors: MIP and genetic information biorecognition-coated QCM sensors.

## 2.1 Molecularly Imprinted Polymer

There has been a noticeable trend toward use of small-molecule analytes in healthcare diagnosis and treatment. Guha and others [30] used molecularly imprinted

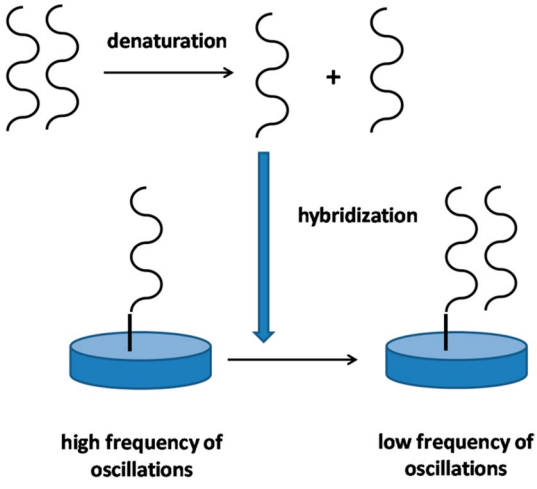


**Fig. 2** The DNA QCM biosensor. Reproduced with permission from Ref. [29]

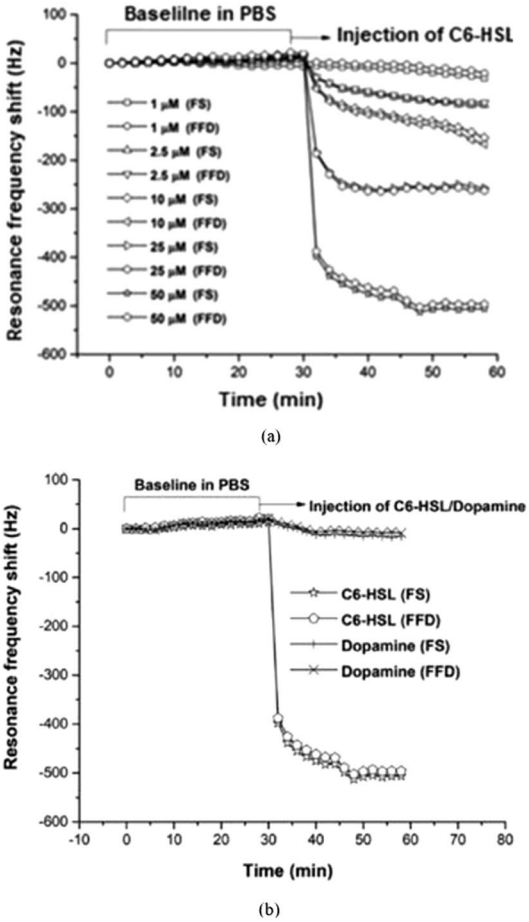


**Fig. 3** **a** The sensor's frequency response after C6-HSL injection. **b** The frequency response to binding with 50 mM of C6-HSL and 50 mM of dopamine on a functionalized QCR. Reproduced with permission from Ref. [30]

polymer nanoparticles (nanoMIPs) technology that mimics biological receptors to examine the sensitivity and label-free detection of *N*-hexanoyl-L-homoserine lactone ($C_6$-HSL), a type of acyl-homoserine lactone (AHL) when deposited over a quartz crystal resonator (QCR). The composite polymer, methacrylic acid monomers, has strong interactions with AHL. We determined the resonant frequency response and dissipation using a fixed frequency drive (FFD).

The nanoMIPs were synthesized using the solid-phase technique, which involves templet immobilization through covalent bonds, polymerization, and affinity separation. Then, the prepared $C_6$-HSL MIP nanoparticles were transferred to the QCR surface.

We then investigated resonant frequency shifts over a $C_6$-HSL concentration range of 1–50 μM. Changes in resonant frequency were determined through a conventional impedance analysis and FFD, as depicted in Fig. 3a. After the injection, both methods produced agreeing results for all $C_6$-HSL concentrations. The frequency shift at the lowest detectable concentration of the proposed system was

about 25 Hz, demonstrating improved sensitivity compared to previously reported methods of detecting $C_6$-HSL. The sensor specificity was examined by using dopamine as a negative control. The frequency shift measurement using the methods mentioned above was also conducted on the specificity experiment and showed an agreement in the results, shown in Fig. 3b. The figure shows that the prepared QCR sensor has a high specificity toward $C_6$-HSL. The proposed QCR nanoMIP sensor can detect and monitor small molecules in real time. MIP-QCM sensors' sensing abilities were previously enhanced through the introduction of compounds.

Navakul et al. [31] produced a graphene oxide (GO)-enhanced MIP QCM sensor for detecting the dengue hemorrhagic fever pathogen [i.e., dengue type 1 virus (DEV-1)]. Dengue hemorrhagic fever (DEF) is a public health problem for tropical and subtropical populations. Multiple infections of different serotypes can damage internal organs. The DENV serotypes need to be quickly detected and identified to prevent adverse health effects. The experiment consisted of two sets of dual electrodes QCM coated with a GO layer, prepared using Hummer's method, and a prepolymer. The GO-MIP film was created by spin coating the polymer over the QCM electrodes. We then pressed a virus template stamp over the coated electrodes. The untreated electrode is referred to as a nonimprinted polymer (GO-NIP). The templet was later removed by stirring in an aqueous solution. The frequency shift of the QCM coated with GO-MIP QCM when it was exposed to DENV-1 was − 1690 Hz for GO-MIP and − 80 for GO-NIP. Another set of QCM sensors, composed of DENV-1-MIP and DENV-1-NI,P were examined. Their frequency responses were − 595 Hz for DENV-1-MIP and − 197 Hz for DENV-1-NIP.

Figure 4 shows the two sets of dual-electrode QCMs. Introduction of GO improved the sensor's response. The GO-MIP sensor displays a linear relationship for a concentration range of $10^0$–$10^3$ pfu/mL; the detection and quantification limits were 0.58 and 1.94 pfu/mL, respectively. Thus, the sensor could detect the virus even at early infection stages. For types of dengue virus serotypes (DENV-1, DENV-2, DENV-3, and DENV-4) with different antigens, MIP selectivity fits well with the differences.

Human serum albumin (HAS) requires continuous monitoring due to its critical metabolic role and since abnormal levels may indicate health problems. Sudjarwo et al. [32] investigated the in situ detection of HSA using a QCM assay with spherical nanoMIPs to produce a single measure that was both sensitive and specific. The nanoMIPs receptors are expected to provide unique sites per particle. The nanoMIPs are synthesized using the solid-phase method. Following the same synthesis procedure, nonimprinted polymer nanoparticles (nanoNIPs) were prepared without glutaraldehyde (GA) and HSA to serve as the reference. One of the QCM's gold dual electrodes was functionalized using HSA solution; the other consisted only of cysteamine and GA. The electrodes' frequency responses were observed following exposure to HAS and bovine serum albumin (BSA). The electrode coated with HAS shown reversible frequency shifts, while the electrode coated with only GA exhibited an irreversible frequency drop of − 238 Hz. After flushing the QCM with PBS, both signals reverted to their respective equilibriums. These results demonstrated the potential for mobilizing HAS on the QCM surface. Additionally, HAS molecules appear to not aggregate on the QCM surface. As shown in Fig. 5, the QCM with

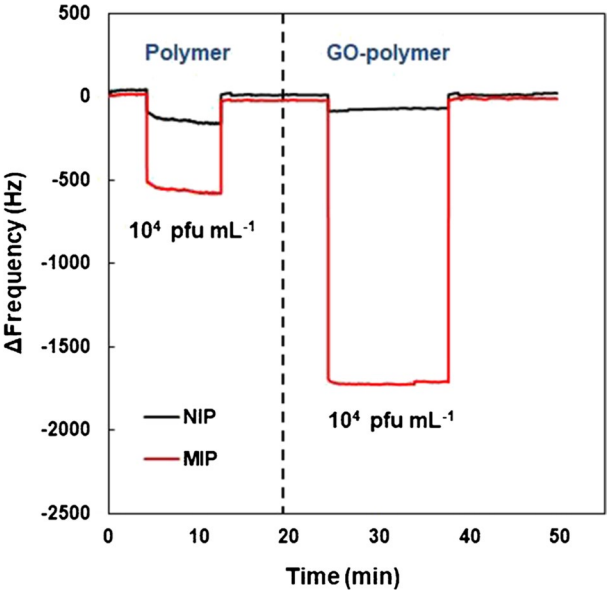


**Fig. 4** The frequency response of the DENV-1-MIP/NIP and GO-DENV-1-MIP/NIP QCMs to GO-DENV-1. Reproduced with permission from Ref. [31]

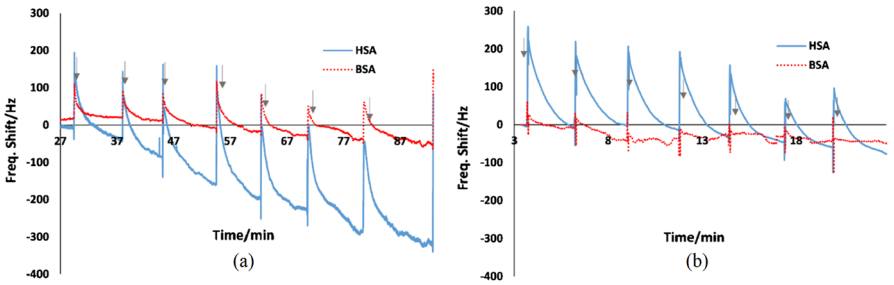


**Fig. 5** The QCM response when upon exposure to **a** nanoMIPs and **b** nanoNIPs. Reproduced with permission from Ref. [32]

nanoMIPs and HSA concentrations between 25 and 750 µg/mL showed frequency shifts from − 44 to 324 Hz. In contrast, nanoNIPs showed frequency shifts from − 13 to − 78 HZ for HSA. These results indicated that the nanoMIPs were roughly 4.2 times more sensitive than the nanoNIPs. The detection and quantification limits of the prepared sensor were 80 nM and 244 nM, respectively. Next, we will discuss use of hydrogel layers for monitoring salivary glucose.

Dou et al. [33] prepared an easy-to-use lab-built QCM coated with a poly(boric acid)-based hydrogel using a UV-pressing technique to monitor salivary glucose. The researchers selected a poly(boric acid)-based hydrogel because of its abundant potential glucose binding sites. The UV-pressing technique consisted of pressing

one of the QCM surfaces against the polymerization solution and with a uniform force. The QCM surface was later irradiated with a 365-nm lamp. The method produced a complete and relatively flat, 420-nm thick layer. The UV pressing detected glucose more efficiently than the spin-coating method. For example, the UV pressing method had a detection limit of 3 mg/L; by comparison, the spin-coating method had a detection limit of 100 mg/L.

In PBS medium, hydrogel-coated QCM sensors demonstrate a frequency shift fluctuation of ~ 13 Hz. A follow-up control experiment failed to produce a 3-(acrylamido) phenylboronic acid (3-APB) frequency response. This indicated that the control hydrogel's frequency shift response was nonsignificant. However, in the case of the boric acid hydrogel, a frequency shift increase was recorded as glucose concentrations were increased 0–160 mg/L, indicating rapid binding between boric acid groups and the glucose molecules. Also, the frequency shift dropped when the experiment was repeated in reverse (the glucose concentration started at 160 and ended at 0 mg/L). Here, the hydrogel's response time to glucose was within 52 s. The control experiment revealed that the 3-APB binds with glucose in solution. Also, the medium's pH affected the hydrogel's binding ability. The experiment found a linear relationship between the frequency shift and the glucose concentration at a pH range of 6.8–7.5. The sensor was tested against artificial saliva to further assess the hydrogel's performance. The results showed similar behavior to the PBS buffer medium; however, the optimum pH value was adjusted to 7.9 to enhance the signal value (since greater pH values resulted in an unstable sensor). The test was repeated 10 times, but no significant changes were observed, thus demonstrating the hydrogel layer's accuracy and stability.

The flavoring, consumer product, and fragrance industries stand to benefit considerably from QCM sensors and their technical advantages. For example, palm oil is used widely throughout these industries given its ability to prevent bacterial and viral infections. Roy et al. [34] fabricated a sealant MIP-coated QCM sensor using the dropcasting method to detect geraniol. Ten sensors were prepared with fixed sealant amounts and varying ratios of acetone, ethanol chloroform, and dichloromethane, then exposed to 100 ppm of geraniol vapor. The coated QCM sensor's response was linear between 5 and 200 ppm. Five palm essential oils (PRO1 to PEO-5) were used for real-time analysis. The maximum frequency shift was observed with POE-1; POE-4 produced the smallest frequency shift.

Next, we discuss use of genetic information as a biorecognition layer over the QCM surface to diagnose genetically determined diseases.

### 2.2 Genetic Information Biorecognition

Genetic information, such as DNA or RNA single-strand short strains, has been used within the biorecognition layer over the QCM surface. During hybridization, there are reduced QCM frequency fluctuations.

PI Reyes et al. [7] functionalized a QCM sensor with ZnO nanotip arrays and increased its sensitivity by exposing the sensing area to UV light for 10 min. Their results demonstrated successful immobilization of ZnO nanotips and hybridization

selectivity. The linker layer appears selective to ZnO nanotips and DNA. The UV exposure lessens the liquid sample consumption by making the sensing area superhydrophilic. The compatibility of the ZnO nanotips with intercellular material makes it a promising candidate for biosensing applications.

The nano-QCM sensor shows a frequency shift that is 10 times higher than a standard QCM. The ZnO nanotips are highly sensitive to intercellular pH changes and can detect enzymatic biochemical reactions. The ZnO nanotips offer an expansive sensing area since their superhydrophilia means less liquid is needed to cover the sensing area. The nano-QCM was calibrated for DNA molecule detection by adding 2 µL nonactivated DNA oligonucleotide.

The researchers used a multilayer transmission line model to imitate the QCM mass loading in a liquid medium. In this model, the acoustic wave propagates through each layer of the QCM device. Impedance is calculated by treating individual layers as a two-port system.

The nanotips are grown on the sensing area through metal–organic chemical vapor deposition (MOCVD). The ZnO nanotips are vertically aligned with a height of 700 nm and 10 nm between the tips. The nanotips were functionalized through the following three steps: First, the nano-QCM was immersed in an *n*-hydroxysuccinimide ester linker solution. After that, the functionalized ZnO surface was immobilized using a single-stranded DNA [35]. Lastly, the functionalized surface was hybridized with a complementary fluorescence-tagged single-stranded DNA.

The frequency response to the mass load of the nano-QCM for the $0^{th}$ step is the nano-QCM before the layering. After that, the first step (linker coating on the nanotips) shows a frequency shift of 1.992 kHz, affirming that 265.606 ng of the linker is present over the functionalized sensing area. In the second step, DNA immobilization was confirmed after a frequency shift of 2.271 kHz, which verified that 303.673 ng of the DNA was present over the nanotips. A 2.271-kHz shift after the last step proved the presence of 264.93 ng of the complementary fluorescence-tagged single-stranded DNA over the sensing area. The uniform frequency shifts suggest that the immobilization and hybridization were uniformly attached to the sensing area. The QCM sensing area was selective to ZnO nanotips. The same three steps were applied on a bare QC. However, no significant frequency shifts were observed.

Due to their selective immobilization and hybridization, ZnO nanotips-QCM sensors show great promise as biological sensors. The proposed nano-QCM has a bright future in enhancing biochemical sensing applications.

Several publications explored nanoparticles as sensing layers in immunosensors. Ortega-Valencia et al. [36] developed a QCM immunosensor with immobilized spherical gold nanoparticles (AuNPs) to detect *Salmonella typhimurium* (*S. Typhimurium*). The researchers studied the influence of AuNP size on frequency measures. The frequency shift sensor was a 6-MHz QCM sensor with two gold electrodes mounted on a circuit board. The researchers examined two different sizes of AuNP: 25 nm and 62 nm. Both were functionalized with cysteinates and immobilized with *S. Typhimurium* monoclonal antibody (AbST). The immobilization process was done through the self-assembled monolayer method. The researchers deposited 5 µL of the immobilized and functionalized AuNPs (Fig. 6). Later, *S. Typhimurium*

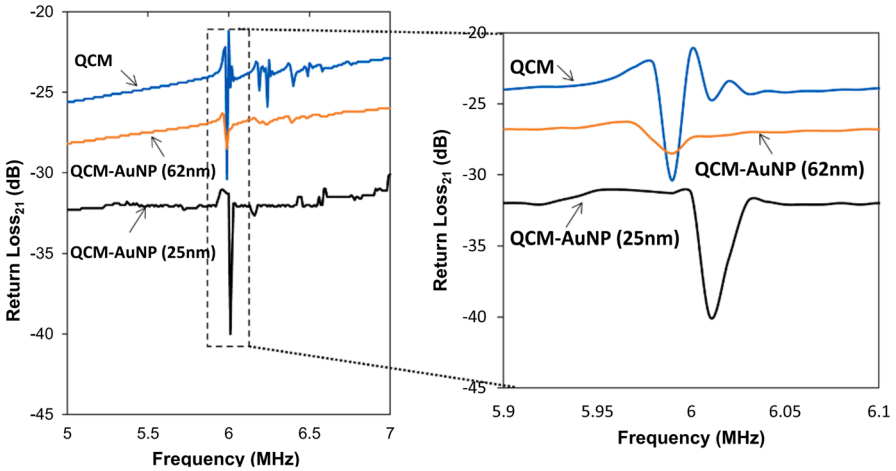


**Fig. 6** The frequency and amplitude responses of the QCM after AuNPs immobilization. Reproduced with permission from Ref. [36]

measurements were conducted with $10^8$ CFU/mL. Coupling of 25-nm AuNPs and the surface enhanced the binding and detection of *S. Typhimurium*. In contrast, coupling of 62-nm AuNPs and the surface reduced the number of *S. Typhimurium* cells. As seen in Fig. 6, the QCM's frequency and amplitude variations with immobilized AuNPs of varied sizes were attributed to *S. Typhimurium*. The 25-nm AuNPs exhibited the highest signal and frequency shifts, suggesting efficient detection of *S. Typhimurium*. It was thought that the larger nanoparticle repulsive force prevented more nanoparticles from binding to the QCM surface. This resulted in low signal enhancement and sensitivity to *S. Typhimurium*.

Nanoparticles and antibody complexes have sparked interest in examining soil protein content. One example is glomalin protein, which has several vital functions. Pohanka and Vlcek [37] fabricated a piezoelectric QCM sensor to detect glomalin protein found in soil. Glomalin protein is created from a widespread fungus and enables the soil to retain water and metals. The protein's biological sensor consists of a layer of immobilized monoclonal mouse hybridoma IgM isotype antibody and iron oxide nanoparticles. The 10-MHz QCM biosensor has a 20-mm quartz disc and 7-mm gold electrodes.

Functionalization took place within a wet chamber. We dissolved 50 µL of monoclonal mouse hybridoma IgM isotype antibody against glomalin in PBS to create a 1-mg/mL concentration which was subsequently applied to the electrodes, which were then left for 12 h in the chamber. The research group prepared iron oxide nanoparticles activated by the carboxylic acid layer.

The soil samples came from the Czech Republic (Branisovice, Kuparovice, and Dubany) and Antarctica. The former is Chernozems—a biologically active and highly fertile area—and samples were taken from depths 0.05–0.15 m. Antarctic soil sampled 0.05–0.10 m from the active later demonstrated less biological activity. The biosensors were calibrated using a soil sample from Dubany, Czech Republic, with

a glomalin content of 3.47±0.19 mg/g. The sensor has detection limit of 2.4 µg/g, and the biosensor showed good sensitivity, which is attributed to the stabilization effect of the iron-oxide nanoparticles. The proposed sensor is suitable for glomalin detection in real samples. The expected glomalin content in fertile farms lies around 2 mg/g.

The antibodies binding caused a 753±44 Hz frequency shift, and the iron oxide nanoparticles binding produced a frequency shift of 958±67 Hz. Albumin affected the oscillation frequency and caused a 132 ± 9 Hz frequency shift. However, the sensitivity reduces after 1 µg/g and above. Interference testing showed that the prepared biosensor is not sensitive to either interference or matrix effects caused by other proteins.

The biosensor was assessed against the standard Bardford methods to analyze 11 soil samples. The standard glomalin content range was 279–3.53 mg/g. The QCM biosensor performed similarly to standard analysis, but with a better detection limit. A new QCM sensor measures a 532±42 Hz frequency changes. The 4- and 8-week biosensors measured 518±39 Hz and 541±45 Hz changes, respectively. They indicated excellent long-term stability under laboratory conditions. Antibody immobilization and iron oxide provides label-free and real sample identification, making the sensor more helpful than standard methods.

Other methods for testing water toxicity were explored using cells' genetic information cells for biorecognition. Lee et al. [38] fabricated a cell-based QCM biosensor for real-time monitoring of water toxicity. They fabricated four QCM sensors attached to a customized printed circuit board to conduct measurements parallel with impedance and frequency shift monitoring. Gill epithelial cells from rainbow trout (RTgill-W1) were used as the biological sensing element. The cells' survivability at room temperature makes RTgill-W1 an excellent candidate for investigating health-threatening concentrations of pentachlorophenol (PCP), a synthetic substance used to preserve fences and power line poles. Short exposure to large amounts of PCP could be fatal. A concentration of 0.526 µM of PCP solution in an L-15 serum-free media was used to investigate water toxicity.

The four QCM sensors comprise 10 MHz quartz crystals inserted between two 0.5-cm electrodes. The culturing well chambers were fabricated over one of the QCM's electrodes. Two sensors were used to conduct the experiment, and the remaining were used to monitor the cell. The cell culture control, abbreviated as QCM1, was not exposed to the PCP solution.

While seeding RTgill-W1cells, the researchers noted a noticeable decrease in impedance and resonant frequency (Fig. 7a, b). This drop was attributed to the mass deposition on the sensor's surface. The frequency decreased further when the cells began to attach to protein molecules and form a monolayer over the sensor's surface. As the layer grew denser, the resonant frequency increased and maintained its stability until the cells began to detach. The frequency reached equilibrium within 24 h. The PCP solution was introduced into the chambers when the cell monolayer covered the electrode.

Figure 7c, d presents the frequency and impedance response following introduction of the PCP solution. The two toxicity chambers' QCMs showed resonance frequencies of 180 Hz and 120 Hz. The slight frequency shift variation is attributed to

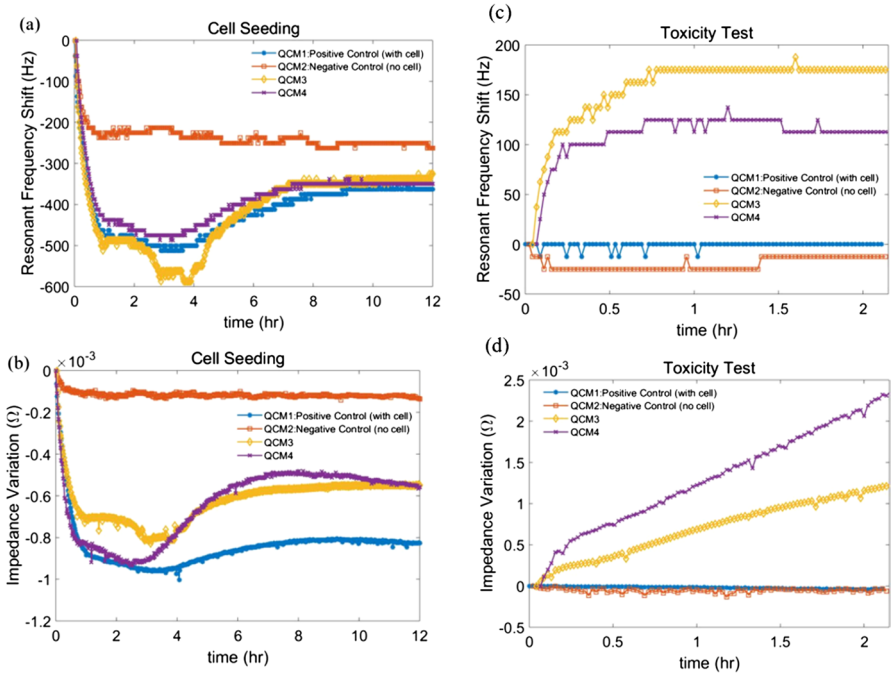


**Fig. 7** **a** The frequency responses of the four sensors. **b** Impedance value variations of the four sensors. **c** The frequency responses of the four sensors to PCP toxicity. **d** The impedance value variation compared to the sensors' initial values. Reproduced with permission from Ref. [38]

the fact that seeding an exact number cells is not feasible. The experiment demonstrated that the cells survived long exposure to PCP. Thus, increases in QCM sensor resonance z is correlated to observations of cell detachments from the sensor's surface. Many factors need to be considered to make the QCM biosensor reusable, including the residual cell material and toxicant that remains on the chip. The prepared QCM biosensor is reusable only if the cleaning process is well-designed.

Continuous work to monitor health-related issues to improve the QCM sensitivity using biorecognition layers as the sensing element has improved the sensors' sensitivity. The need for sensitive, rapid, and point-of-care tests with minimal sample pretreatment has risen due to the worldwide spread of SARS-CoV-2, the respiratory pathogen responsible for the 2019 coronavirus pandemic (COVID-19). The virus is a positive single-stranded RNA consisting of a spike, envelope, membrane, and nucleocapsid protein (N-protein). Forinová et al. [39] fabricated an antifouling QCM (A-QCM) biosensor for detecting COVID-19 in a complex within 20 min without sample pretreatment. The A-QCM is a 10 MHz resonator inserted between two gold electrodes. The sensor was modified by application of a viscoelastic coating sensitive to the target in a complex environment. Polymer brushes were prepared and adhered to the electrodes' surfaces by adding an alkanethiol layer. Later, the sensors were functionalized with human cell-produced antibodies against COVID-19 nucleocapsid protein.

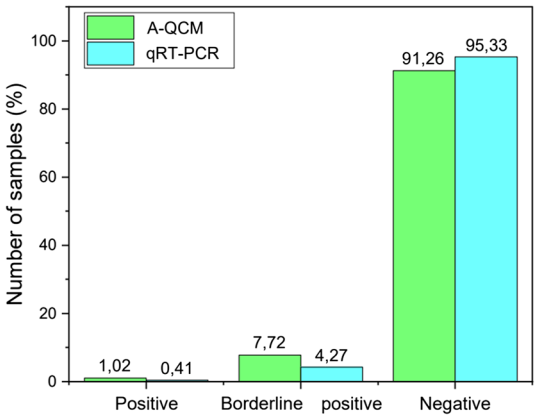


**Fig. 8** A-QCM and qRT-PCR results. Reproduced with permission from Ref. [39]

Using a one-step sensor format, the researchers analyzed SARS-CoV-2, Hepatitis A virus, Escherichia coli, and other swab samples in real-time using an A-QCM sensor. The mass variations were calculated from the A-QCM's response in a PBS buffer before and after sample deposition. The biosensor functionalized surface was exposed to virus samples at 102–106 pfu/mL concentrations. The sensor's detection limit was $6.7\times10^3$ PFU/mL.

The researchers used qRT-PCR and A-QCM to analyze 492 samples collected from public transportation vehicles; Fig. 8 summarizes the results. The two methods' partial agreement is attributed to the fact that qRT-PCR focuses on the number of viral vRNA copies, while the A-QCM sensor focuses on detecting the viral N-proteins. The sensor can deliver accurate results quickly from complex samples.

Jin et al. [40] exploited an amorphous metal–organic cage-based solid (aMOC) and signal probe DNA complex to enhance the delectability of target miRNA (let-7a). MiRNAs are a group of noncoding small molecules that help regulate gene expression. A thiol-modified capture probe DNA (cpDNA) is assembled over a QCM with gold electrodes to hybridize with the target miRNA (tmiRNA), creating double-strand assemblies on the QCM while forming open base sequence sites on the surface. Signal probe DNA (spDNA) and aMOC complexes were applied to bind with the QCM to function as a signal intensifier, identifying undetectable tmiRNA. An optimum concentrations of aMOC was 10 µL spDNA was 1 mL. The authors observed a slight frequency shift of 6 Hz when they tested the sensor using 50 nM of let-7a (tmiRNA) without adding the complex to test its amplification ability. However, an enormous frequency shift of ~ 86 Hz was observed when the spDNA@aMOC-2 complex was added to the QCM sensor at the same concentration as let-7a. The frequency responses of the aMOC02@spDNA coated QCM sensor were recorded at different concentrations (0 fM, 1 fM, 10 fM, 100 fM, 1 pM, 10 pM, 100 pm, 1 nM, and 50 nM). The frequency shift decreased as the tmiRNA concentration increased from 1 fM to 50 nM. The detection limit was 247aM. The specificity of detecting let-7a was tested against 50 nM miRNA of one-base mismatched strands (let-7c and let-7e) and a two-base mismatched strand (let-7b). Significant selectivity favoring the target let-7a was found when the researchers experimented

with different miRNAs. The sensor's accuracy and repeatability were tested under different concentrations of the target miRNA, with each concentration tested five times. The researchers found the prepared sensor to be accurate and feature good repeatability; the recovery rate was between 94 and 116. The prepared sensor could be used clinically for detecting complex biological samples. The authors confirmed sensor's ability to detect let-7a of various concentrations (1fM, 10 pm, and 50 nM) in diluted bovine serum, thus confirming their clinical applicability.

Thanaporn et al. used continuous flow technology and QCM sensors to investigate the kinetic binding interactions between two elements derived from human blood using continuous flow QCM sensor technology [41]. Specifically, their studied the kinetic binding interactions between exomeres with sizes < 50 nm and exosomes with sizes ranging between 50 and 150 nm among extracellular vesicles (EV) subpopulations, named according to their target tetraspanin surface proteins $CD9^+$, $CD63^+$, and $CD81^+$ and extracted from human plasma. The authors examined the subpopulations against four affinities monoclonal antitetraspanin antibody ligands (anti-CD9, anti-CD63, and anti-CD81); the recombinant was ICAM-1. The amine coupling was utilized to immobilize the antibodies and the ICAM-1 separately on the surface of an LNB-carboxyl sensor. The two-site interaction model was used for data analysis. The study was conducted under an EV subpopulation injection flow rate of 25 µL/min at 37 $^{O}$C.

The sensor was processed and analyzed using the Adaptive Interaction Distribution Algorithm to view the number of interaction sites with association $k_a$ and dissociation $k_d$ constant rates and binding. The Anti-CD9 and anti-CD63 interaction site 1 was the main contributor when both antibodies were investigated—separately—against the exomere- and exome-sized EVs as the ligands were immobilized over the QCM chip. The authors further observed EV interactions against the anti-CD-81 ligand. All exomere-sized EVs exhibited similar rate constants toward the ligand. Most EVs and the ligand interactions had a dissociation constant $k_d$ over $10^{-9}$ M. The $CD63^+$ exomere had the strongest affinity with all the antibodies, suggesting that $CD63^+$ contains surface CD9, CD81, and CD63. Exomere- and exosome-sized EVs had an average $k_d$ value of $10^{-14}$ M for Site 1 and $10^{-10}$ M for Site 2. With the highest interaction being between the $CD63^+$ and the anti- CD63. Most site 1 interactions demonstrated an affinity in the M range. The fM range binding might be attributed to multivalent ligand binding. All the ligands used in the experiment showed excellent ability to be utilized as immunoaffinity isolation and immunosensors. When the researchers examined interactions between EVs and ICAM-1, ICAM-1 displayed the same trends as the antibodies; however, the antibodies had higher affinity than the ICAM-1. This could be attributed to the strong and specific binding of monoclonal antibodies. The dissociation constant rate for ICAM-1 and EVs interaction examined in this study was higher than the $k_d$ value reported in the literature, potentially because of receptors on the EV's surface.

A viscous protein layer formed over self-assembled monolayers (SAMs) was investigated by Mondarte et al. [42] in a BSA-crowded biological environment. The researchers used two SAM layers—one composed of 1-octane thiol (C8 SAM) and the second composed of zwitterionic sulfobetaine (SB)-terminated alkanethiol (SB SAM). The SAMs layers were deposited on an atomic force microscope and a

QCM (using an energy dissipation technique, QCD-D) surface by immersion. As for the crowded environments, the research team tested a single-component environment consisting of BSA and a multicomponent environment consisting of various concentrations of fetal bovine serum (FBS) protein solution. The QCM-D was prepared by adding a Ge/Au bilayer film through thermal evaporation. The QCM-D frequency shifts were recorded to establish a baseline in the PBS environment. Then, the researchers introduced the crowded environment and restabilizing the QCM-D's signal. The amount of the adsorbates that remained after rinsing (referred to as the *areal mass density*), was used to evaluate the protein's surface fouling. The areal mass could be derived from the QCM-D's frequency shift. The rigidity of the adlayer remainders influenced energy dissipation (rigid adlayers induced less dissipation). For the C8 SAMs, the 80 mg/mL BSA solution showed high mass adsorption compared to the 5 mg/mL BSA solution; this implies that proteins progressively accumulate at the interface with increasing serum concentrations. The authors also examined 10% and 50% of FBS solution in BSA. However, the various concentrations had no significant effect on the adlayer's mass and the rigidity. This limited the adsorbates regardless of the number of crowders in the bulk solution because protein accumulation was limited by larger and denaturation-resistant molecules. The QCM-D measurements revealed that SB SAMs possess an antifouling property against BSA solution. On the other hand, the 50% FBS showed 1.6 times more mass adsorption than C8 SAM. Interface proteins release water molecules when denatured; this decreases frequency shifts and limits energy dissipation. The SB SAM has a more significant denaturation, which explains observed adsorbtion rates.

The dissipation signals vs. the frequency response plots for the sensor before and after rinsing with PBS were used to understand the SAM layer formation. The plots' steepness reflects the introduction of the crowder environment, the adsorption process, and the final rinsing procedure.

Prerinsing, the C8 SAM plot was curved with the frequency shift and dissipation induced by the bulk liquid and simultaneous adlayer formation after solution introduction. After rinsing, however, the removal of a more dissipative viscous layer appeared in the plot as a steeper slope.

In the 50% FBS environment, three adsorption stages were observed before rinsing (BR1, BR2, and BR3) and two after rinsing (AR1, AR2). From the plots for the two SAMs at the two environments shown in Fig. 9, the BR1 curve with the C8 SAM (Fig. 9a), a simultaneous bulk effect and quick and mobile protein molecule adsorption were observed. In the BR2 stage, water molecules were slowly released because of denaturation of the adsorbed protein molecules. The final stage, BR3, was prolonged and featured a spiraling plot that was hard to interpret. Once larger molecules reached the surface, they partially replaced the initial adsorbates. This process terminated formation of multilayers near equilibrium (the Vroman effect). The steepness of the plot (AR1) indicates that the first molecules released after rinsing were large. The slight desorption at 300 μL/min demonstrated the layer's rigidity secondary to serum molecule denaturation. The flat plot for the after-rinsing AR2 stage at 600 and 900 μL/min implies that no further desorption has occurred (Fig. 9b).

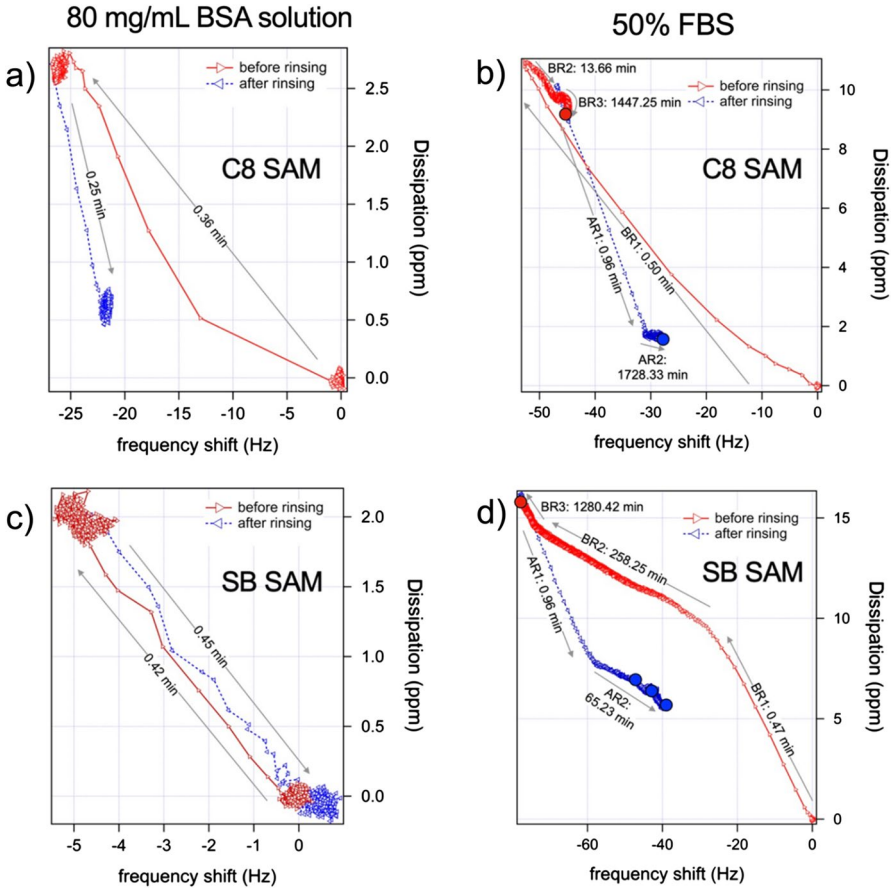


**Fig. 9** The dissipation versus frequency plot for the C8 SAM in (a) 80 mg/mL BSA solution and ( **b**) 50% FBS solution. The dissipation versus frequency plots for the SB SAM (**c**) 80 mg/mL BSA solution and in (**d**) 50% FBS solution. Reproduced with permission from Ref. [42]

The SB SAM was highly resistant to the BSA solution, as depicted in the linear plot before and after rinsing (Fig. 9c). These findings imply that the frequency and dissipation changes were attributable to the bulk 80 mg/mL BSA solution (stage AR1).

The plot in Fig. 9d for the 50% FBS environment shows that the dissipation shifts caused by the bulk solution (BR1) induced delayed adsorption (shown in BR2). The comparable slopes substantiate the results before and after the rinsing stages, BR1 and AR1, confirmed by their comparable slopes. The Vroman effect could explain the long-standing BR3 stage. The similar AR2 and BR2 slopes indicate that the small-molecule adsorbed layer is rigid (after stage AR1 exposure). Sb SAM's protein resistance to the FBS solution was demonstrated by reductions in the residual adsorbed mass as the rinsing rate increases.

It is vital to analyze human blood components such as hemoglobin (HB), white blood cells (WBCs), red blood cells (RBCs), and plasma to diagnose many diseases such as hemophilia and anemia. Hossain et al. [43] fabricated a hollow-core photonic crystal fiber (WCPCF) biosensor using 3D printing techniques. The WCPCF was constructed from Zeonex fibers because of their constant refractive index (RI) of 1.53 through the targeted regime (in THz). The researchers used the COMSOL Multiphysics simulation tool to construct the sensors considering a 3.5-mm diameter optical fiber. By experimenting with the widths and lengths of six different rectangular cores, they found the highest sensitivity a width of 500 µm and a length of 700 µm. Although widths of 510 µm and length of 710 µm showed high sensitivity, these dimensions would complicate the fabrication process. They found a proportional relationship between frequency and light power confinement through the core, thereby increasing the sensor's relative sensitivity. The cladding hole width affects the core power fraction by fixing the hole lengths. The proposed design successfully detected the blood components with an approximate relative sensitivity of 89.14% for water, 90.48% for plasma, 91.25% for WBCs, 92.41% for HB, and 93.50% for RBCs at 2 THz.

## 3 Chemical Sensors

Rianjanu et al. [44] discussed the various applications of nanofiber-coated QCM gas sensors. Polymers and semiconductors are used to prepare electrospun nanofibers. Fibrous materials with large surface areas, inherent porous structures, and 3D architecture are obtained through electrospinning. Their unique 3D design enhances the active site area, affecting sensor response. The material's porous nature creates channel-like paths for targeted gas molecule diffusion. Another factor influencing a sensor's performance is the number of active sites and analyte molecule interactions. These interactions cause QCM frequency fluctuations, which are later designated the sensor signal. Nanofibers have numerous applications, including energy storage, filters, and sensors and have potential as a QCM sensor coating since no prior activation is needed to capture analytes. The nanofiber-coated QCM's sensitivity is mainly affected by the fiber's structure and morphology. In contrast, the nanofibers' architecture and composition affects selectivity. The three categories of unmodified and overlaid metal oxide nanofibers are characterized based on their architecture.

Unmodified polymer nanofibers are used as a single or mixed polymer solution without further modifications to function as a sensing layer over the QCM's surface. The composite polymer component ratio is important and requires optimization. The mixed solution contains two essential precursors: a viscosity modifier to facilitate electrospinning and a sensing material. Although simple, electrospinning does not work with all polymer solutions. For example, ammonia detection using a nanofiber-coated QCM sensor could have a detection limit reaching the ppb level. Also, depending on the targeted gas, limits of detection fall in the range of 23–50 ppm. Introducing acids as doping agents when preparing nanofibers noticeably enhanced their sensing abilities. For example, boric acid mixed with polyvinyl acetate (PVAc) was twice as sensitive as undoped polyvinyl acetate (PVAc). Additionally, organic

acids like citric acid increased the PVAc sensitivity to up to 2.95 Hz/ppm and produced a nanofiber that was highly selective to ammonia vapor. The detection of formaldehyde using a nanofiber-coated QCM revealed that polymers with excessive amine groups influence the sensor's sensitivity to formaldehyde.

The electrospinning constraint that might arise from some polymer solutions has been overcome by alternating use of drop casting and dip coating. The overlaid material will significantly influence a sensor's sensitivity. However, it should not change the fiber's structure in order to preserve the fiber's high surface area. The overlay should be insoluble and retain its high mechanical characteristics. Typical polymers used as overlaying material possess a selective adsorption quality. Polyacrylonitrile (PAN) overlaid with polyvinyl amine (PVAm) polymer can detect formaldehyde with a 500 ppb detection limit. As for ammonia detection, a cellulose acetate overlaid with polyethyleneimine polymer exhibited a high selectivity toward ammonia, and its sensitivity reached 0.9 Hz/ppm. Nanofiber-net-binary (NNB) membranes resemble overlaid nanofibers and are constructed by modifying small nanofiber web networks within the structure (much like a 2D spider web). The NNB architecture could be obtained from different collectors' shapes. Formaldehyde detection QCM sensors with polyethyleneimine-modified chitosan NNB membranes had a sensitivity of up to 0.172 Hz/ppm. Metal oxide nanofibers are used as gas sensors because of their high surface roughness. Metal oxide is a preferred layer because of its thermal and chemical stability, low cost, and simple operating principle. Metal oxide nanofibers are created via in situ incorporation of the precursor; then, the prepared nanofibers are dipped into the precursor. The polymer needs to be fully evaporated; thus, calcination is needed for nanofiber production. The weak physical interactions between the nanofibers' oxygen-active sites and the targeted gas molecules are advantageous since QCM sensors favor weak physical adsorption interactions. Palladium oxide nanofibers can detect high mercury vapor concentrations up to 10.55 mg/m$^3$.

### 3.1 Polymer-Based

Kuwat et al. [8] fabricated a chitosan polymer-coated QCM for alcohol vapor analysis. Chitosan is a widely used natural polysaccharide polymer with excellent film-forming capability, high mechanical strength, hydrophilicity, and antibacterial properties. Detecting volatile organic compounds (VOCs) is important for environmental protection, human health, and quality control efforts. Real-time monitoring of alcohol in air is of immense importance, as long-term exposure to 0.15–0.30 mg/L VOC concentrations can be fatal.

The researchers examined the sensor's sensitivity against n-amyl alcohol, isoamyl alcohol, n-propanol, and ethanol. The QCM was coated with an L-cysteine monolayer using a self-assembly method. The QCM consisted of a 10 MHz AT-cut quartz attached to a 6-mm diameter gold electrode. Layer deposition over the QCM was confirmed through frequency variations. There was an observed decrease in the resonant frequency shift of 176.5 Hz after the L-cysteine layer,

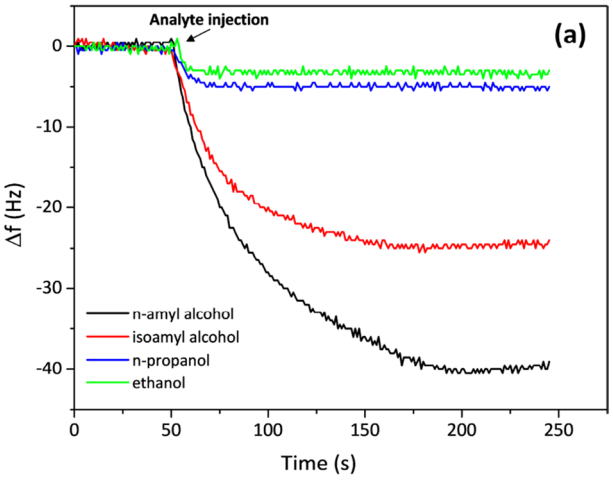


**Fig. 10** The frequency shift response of the chitosan-QCM sensor after exposure to 7 mg/L of alcohol vapor. Reproduced with permission from Ref. [8]

571.5 Hz after the glutaraldehyde layer, and 12,750.5 Hz after the chitosan layer. According to Sauerbrey's equation, the mass loading over the chitosan-QCM exposed to 7 mg/L vapor of each analyte was estimated to be 54.1 ng for n-amyl alcohol, 27.7 ng for isoamyl alcohol, 5.7 ng for n-propanol, and 3.4 ng for ethanol.

The four analytes were investigated to study the QCM's frequency response following separate exposure to 7 mg/L of n-amyl alcohol, isoamyl alcohol, n-propanol, and ethanol. The analytes rapidly declined for a few seconds, then plateaued after 100 s. As seen in Fig. 10, N-amyl alcohol had the highest resonant frequency shift, reaching 39 Hz. In contrast, ethanol scored the lowest value (3 Hz). Isoamyl alcohol and n-propanol frequency shifts were 25 and 5 Hz, respectively.

The researchers repeated the experiment with varying concentrations of the same analytes and acetone. N-amyl alcohol showed the highest sensitivity, and ethanol the lowest. The correlation coefficient of the chitosan-QCM for all the test samples was linear and reproducible. The sensitivity might be affected by the analytes' molecular weights; however, n-amyl alcohol's selectivity is attributed to its linear structure. The n-amyl alcohol had the longest response time, and ethanol had the lowest. The high sensitivity and long response time of n-amyl alcohol could be explained since high vapor pressure requires a short time response time.

The high-frequency response of chitosan-QCM is believed to result from the hydrogen bond that forms between the alcohol molecule's (–OH) and chitosan's hydroxyl groups. The proposed sensor demonstrated a relatively stable frequency shift after 10 days of continuous measurements.

Gas chromatography (GC) can also be used to detect VOC gases. Successful experiments showed that GC incorporated with QCM gas sensors demonstrates excellent sensitivity to VOCs. Son et al. [45] built a hybrid GC microcolumn and QCM gas sensor for accurate sensing and identification of VOC gases. GO flakes

were dropped onto the gold electrode of a 9 MHz QCM sensor to act as the adsorbing layer and enhance sensitivity. Then, a PDMS polymer was cast onto a prepatterned photoresist. Then the mold was later transferred from the photoresist onto the QCM gold electrode.

The researchers compared QCM without microcolumns (CGO-QCM) and the prepared microcolumn GO-coated QCM (MGO-QCM). Differences in gas diffusion rates were utilized for selective gas identification. The time-dependent adsorption behaviors of ethanol, acetone, and hexane were examined at injection rates of 2.4 mL/min for 5 min, then flushed for 5 min. The MGO-QCM sensor with a cross-sectional area of 100 $\mu m^2$ displayed a decreased response because the PDMS microcolumns cover parts of the QCM's surface. The mean adsorption time constants for ethanol, acetone and hexane for CGO-QCM were 71.9, 94.5, and 78.4 s, respectively. MGO-QCM had 100.7, 192.8, and 95.5 s for ethanol, acetone, and hexane, respectively. The different time-constant parameters could be used to identify unknown gas and provide sensing selectivity.

Although chitosan is a polymer used as a sensing layer, other polymers could increase the risk of polluting the environment due to their slow photodegradation. The wide use of polystyrene (PS) in industries such as electronics, medicine, and aerospace engineering, coupled with inadequate recycling measures, makes it vital to discuss PS recycling methods to prevent environmental pollution. PS features slow photodegradation; therefore, if its lifecycle could be extended through recycling, PS waste would be immensely reduced. The main goal of PS recycling is to reduce the polymer's carbon footprint. Alodhayb [46] examined the effect of UV light on QCM coated with PS thin films. The QCM featured 8-mm diameter silver electrodes and a resonant frequency ~ 4 MHz. A 1 μm thin film was obtained by mixing PS pallets with anhydrous toluene (50 μL). This solution was used to spin coat the electrodes. The sensor's stability was examined by screening the uncoated QCM for 14 h. The coated QCM displayed a resonant frequency drop of ~ 22.2 kHz, attributed to the increase in mass associated with the thin film. The resonant frequency shift also demonstrated good coupling between the thin film and the sensor. Photodegradation of the thin film measures was implemented by irradiating the sensor with a 365-nm UV light at an optical intensity of 1.5 mW. The experiment was divided into three segments. Measurements of the resonant frequency pre and postdeposition are shown in Fig. 11. After being irradiated for 7 h during the first segment, the researchers observed a significant resonant frequency shift of ~ 155 Hz. The shift was attributed to reductions in the film's molecular weight by photodegradation. In the next segment, the irradiation was paused for 7 h, showing that the thin film's integrity remained intact. The final segment featured another 10 h of irradiation. During this time, the slow PS photodegradation continued, and a resonant frequency shift of about 100 Hz was recorded.

The high resonant frequency variations of the coated compared to the uncoated QCM produced a high standard deviation ($\delta_{coated} = 74$ and $\delta_{uncoated} = 17$), indicating instability. This instability could be related to fluctuations in film thickness or other factors. The quality factor (Q) changed insignificantly before and after UV irradiation. Thus, resonant frequency changes are mainly due to polymer's UV degradation and viscoelastic behavior.

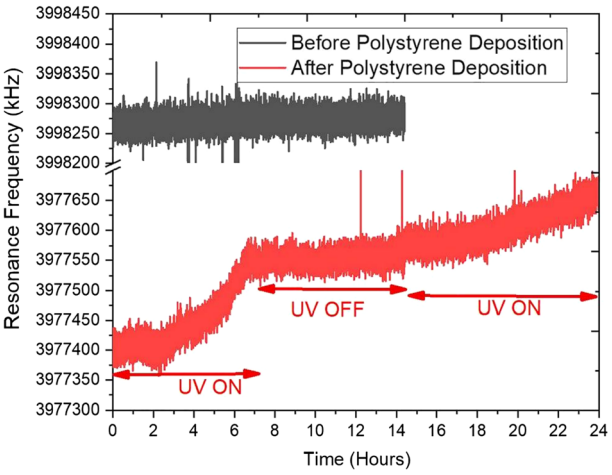


**Fig. 11** The frequency response of the QCM sensor pre and postpolystyrene deposition over time. Reproduced with permission from Ref. [46]

### 3.2 Metal–Organic Frameworks

Metal–organic frameworks (MOFs) are self-assembled porous materials that feature a uniform and periodic inorganic metal center structure (secondary building units-SBUs) and bridging organic linkers called ligands. Ideally, MOFs could be predicted by selecting the ligand and SBUs to achieve the desired structure. MOFs are used to create QCM sensors because of their porosity and physical and chemical characteristics can be changed by simply changing the ligands and metal centers used. Wang [47] described MOFs as comprising a sensing layer over a QCM sensor for gas detection. The MOFs classifications are categorized based on the SBUs' functional groups, such as azolate, carboxylate, and other ligand-based MOFs.

Humidity acts as a constant constraint on MOF selectivity. The relative humidity (RH) approach is used to determine ambient humidity. RH refers to the percent water vapor in the air against the saturated water vapor pressure at the same temperature. A wide range of RH can be created using different types of saturated saline. A QCM coated with HKUST-1(a carboxylate-based MOF) through a drop-casting method has been used as a sensing layer over a QCM surface. The coated sensor preferred for humidity sensing due to its high energy adsorption. The coated sensor showed a sizable frequency shift response compared to an uncoated QCM sensor under 22% to 69% RH levels. Other techniques, such as spin coating, were used to fabricate carbon nanotubes. The spin-coating technique was used to fabricate HKUST-1 (CNT-HKUST-1) composite film. The researchers examined coated and uncoated QCM sensors and found that HKUST-1 with 0.5 mg CNT had the highest sensitivity to humidity: − 141 Hz/1%RH which is 230% higher than HKUST-1 alone. The different sensitivities were believed to be caused by the different crystal sizes which could affect water sorption.

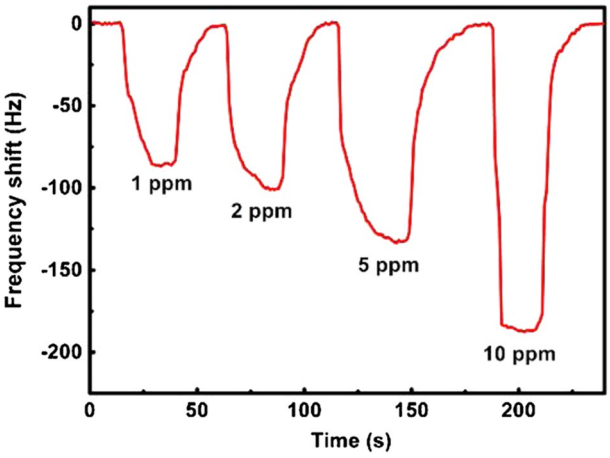


**Fig. 12** The prepared sensor's response and recovery time response to benzene vapor concentrations of 1–10 ppm. Reproduced with permission from Ref. [48]

Ma et al. [48] developed a metal–organic framework (MOF) coated QCM sensor to detect benzene vapor. Long-term exposure to benzene, toluene, ethylbenzene, and xylene is harmful. Because benzene cannot be expelled from the human body through oxidization, it accumulates and can lead to cancer. MOFs are considered a suitable match for QCM sensors due to their high specific surface area and numerous adsorption sites. In addition, MOF tunable port size determines its selectivity to gas molecules.

Four MOF coatings (MOF-14, HKUST-1, MOF-177, and MOF-74.) were prepared to investigate the proposed sensor's sensitivity to benzene. A10 MHz QCM with silver electrodes was cleaned prior to deposition of MOF coating using the dropcasting method. The prepared MOF-coated QCM sensors were exposed to benzene vapor at a concentration of 80 ppm at room temperature. The MOF-14-coated QCM showed the greatest frequency shift of 1200 Hz. MOF-177, HKUST-1, and MOF-74 had lesser frequency shifts of 743, 480, and 200 Hz, respectively. The researchers concluded that the ligand's benzene rings had a greater effect on sensor sensitivity than the central metal. The MOF-14 was considered superior to the other coatings since $Cu^{2+}$ served as the central metal and it featured more benzene rings.

The selectivity of the MOF-14 coating to benzene was investigated by exposing the sensor to seven gas vapors (acetone, methanal, methanol, ethanol, toluene, xylene, and ethylbenzene). The MOF-14-coated QCM showed excellent selectivity to benzene because of the strong $\pi-\pi$ interaction and Lewis's acidity sites.

There has been a noticeable frequency shift of 85 Hz per 1 ppm of benzene concentration; Fig. 12 shows the frequency response of the MOF-14-coated QCM to benzene concentrations of 1–10 ppm. The sensor has a fast response time of 10 s. A second exposure to benzene vapor revealed that a linear frequency response was feasible when the MOF-14 coating was exposed to benzene concentrations below 10 ppm. Judging by the observed linearity, the detection limit was estimated at 150 ppb. Although the MOF-14-coated QCM sensor produced stable and

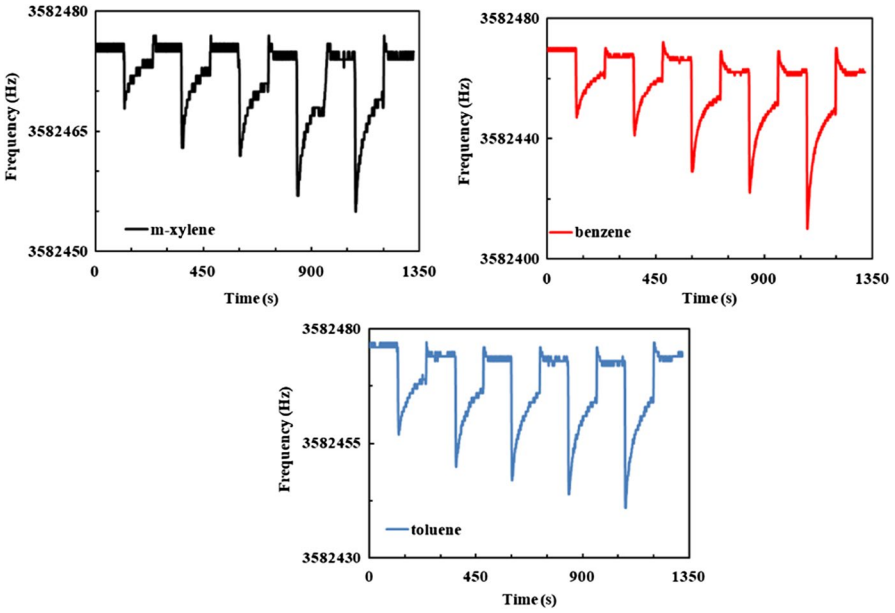


**Fig. 13** The frequency response of the sensor to m-xylene (black), benzene (red), and toluene (blue). (Color figure online) Reproduced with permission from Ref. [49]

reproducible results, further modifications are required mitigate humidity's effects on the signal.

### 3.3 Macrocycle Coating

Due to their cavity size and cyclical structure, macrocycle molecules serve as an ideal sensing layer. Zeybek et al. [49] utilized a chiral calix[4]arene macrocycle material as a sensing element coating over a 3.5-MHz QCM sensor for detecting BTX hydrocarbons (benzene, toluene, and xylene) vapors. Nine film layers were deposited over the QCM electrode using the Langmuir–Blodget technique. The research group observed linearity between the number of deposited layers and the frequency shift if equal masses were deposited in each layer. The deposited mass was estimated to be 2206.65 ng per monolayer. The researchers monitored the coated-QCM frequency response to different concentrations of benzene, toluene, and m-xylene vapors, as shown in Fig. 13. Here, the frequency shift increases in proportion to the percent concentration of aromatic hydrocarbon vapors. Benzene showed the highest frequency shift, m-xylene showed the lowest, and toluene fell between the two. These results were attributed to the BTX vapor's low molecular pressure and high molar volume which allowed it to quickly diffuse into the film. This made the coated QCM highly responsive, sensitive, and selective for various concentrations of benzene vapor.

Shaban and Eddaif [50] studied the effectiveness of a QCM chemo sensor with four resorcinarene derivative films, C-dec-9-en-1-ylcalix[4]resorcinarene (ionophore I); C-undecylcalix[4]resorcinarene (ionophore II); C-dec-9-enylcalix[4]resorcinarene-O-(S-)-α-methylbenzylamine (ionophore III); and C-dec-9-enylcalix[4]resorcinarene-O-(R +)-α-methylbenzylamine (ionophore IV), for detecting heavy metals (HMs) (Copper- $Cu^{2+}$, lead- $Pb^{2+}$, mercury- $Hg^{2}$ and cadmium- $Cd^{2+}$) found in aqueous solutions via in situ QCM-impedance measurements. The experiment occurred in a flow cell under 40 µL. The four coatings were synthesized through condensation reactions at different concentrations of 5, 25, 250, 500, and 1000 ppm for the aforementioned HM ions. The coatings were dropcasted over a 5 MHz QCM with a 14-mm diameter and gold electrodes. The layers' cavities on the sensor's surface bound to the molecules because of charge transfer. An uncoated QCM reference showed no interaction between the HM and the QCM surface. These results suggested that frequency shifts depended on ion concentrations. Initially, all four coatings detected HM ions with different sensitivities. However, QCM coated with ionophores (I) and (II) was best at detecting HMs, with detection limits of 0.32; 0.56; 0.37; 0.89 ppm for ionophore (I), and 1.63; 0.18; 0.76; 0.2 ppm for ionophore (II) for the $Cd^{2+}$, $Cu^{2+}$, $Hg^{2+}$, and $Pb^{2+}$, respectively. In contrast, the other two coatings were only moderately sensitive to HM ions.

Eddaif and others [51] synthesized two novel compounds from enantiomeric macrocycles bearing chiral moieties, denoted as compounds B (C-dec-9-enylcalix[4]resorcinarene-O-(S-)-*α*-met hylbenzylamine) and C (C-dec-9-enylcalix[4]resorcinarene-O-(R +)-*α*-methylbenzylamine). The two compounds were exploited as a sensing layer over QCM sensors to detect lead(II) ions in aqueous solutions. HM ions in water must be detected and removed due to the immense risk they pose to human health.

Experimentally, the compounds were dropcasted on the Au-surface of the QCM (QCM with impedance measurements) using various concentrations of lead ions ($Pb^{2+}$; 5, 25, 250, 500, and 1000 ppm) in aqueous solutions. The prepared sensor's frequency response to $Pb^{2+}$ exposure was recorded for the two compounds. From Fig. 14a, There was a noticeable frequency variation of − 23 Hz for compound C. In contrast, compound B (Fig. 14b) showed a frequency variation of − 10 Hz at 1000 ppm because of the nitrogen atoms contained in both calixresorcinarene derivatives. A dissipation examination revealed that compound B displays rigid characteristics for low lead concentrations. However, viscoelastic behaviors appear following exposure to 500- and 1000-ppm $Pb^{2+}$ concentrations. Compound C had rigid characteristics as per Sauerbrey's estimation and demonstrated compound C's superiority.

### 3.4 Composite Oxide Coating

Formaldehyde ($HC_2O$) is widely used in various chemical compounds and by industries like wood processing and construction. Unfortunately, prolonged formaldehyde exposure can damage lungs and is associated with many other health risks.

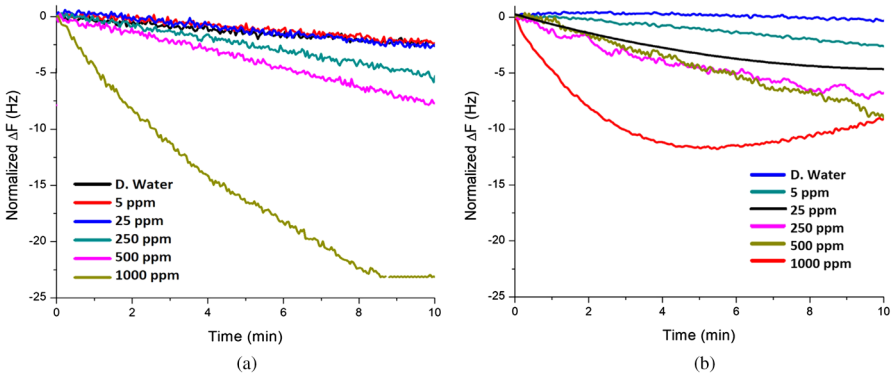


**Fig. 14** The frequency response against lead ions concentrations in solutions (starting with deionized water and up to 1000 ppm) of the QCM coated with **a** compound C and **b** compound B. Reproduced with permission from Ref. [51]

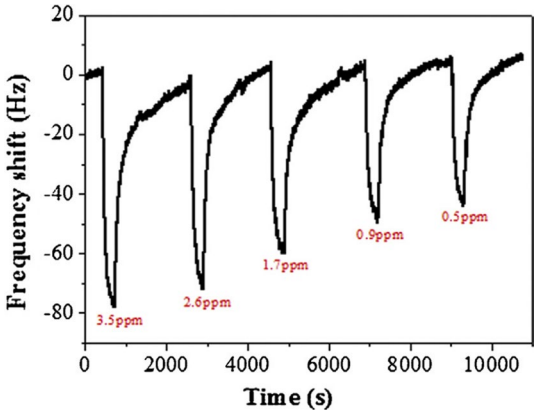


**Fig. 15** The frequency response of the functionalized QCM upon exposure to different formaldehyde gas concentrations. Reproduced with permission from Ref. [53]

Consequently, the World Health Organization (WHO) designated a $HC_2O$ exposure limit of 80 ppb. Therefore, in situ and real-time monitoring devices are urgently needed for detecting $H_2CO$ leaks. Yang and He [52] optimized the sensitivity of their QCM sensors by coating the surface with GO for formaldehyde detection. A large number of oxygen atoms in the form of functional groups in GO aid in hydrogen bonding. The experiment chamber was inside an incubator maintained at 20 °C. The reversible adsorption–desorption process via hydrogen bonding makes the functionalized QCM reproducible, essential for chemical sensors.

GO was dropped over the sensing area of a 5-mm QCM silver electrode via micro syringe. We compared the nonfunctionalized silver-coated QCM to the proposed functionalized QCM to study its sensitivity to formaldehyde concentrations in the range of 0.5–3.5 ppm. The bare QCM did not react to the introduction of $H_2CO$. Thus, the prepared QCM sensor has a better sensitivity to $H_2CO$.

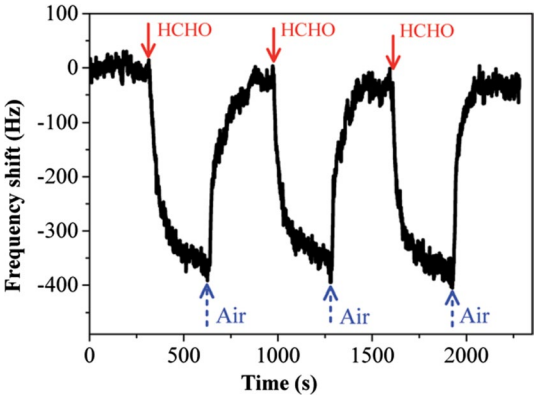


**Fig. 16** The frequency shift of the copper–manganese coated QCM sensor to three cycles of a 1.7 ppm formaldehyde concentration followed by flushing. Reproduced with permission from Ref. [53]

When $H_2CO$ concentrations of 3.5 ppm, 2.6 ppm, 1.7 ppm, and 0.9 ppm were injected into the chamber, the QCM frequency response decreased as the concentration decreased. The plot in Fig. 15 displays the functionalized QCM sensor response following exposure to 3.5, 2.6, 1.7, 0.9, and 0.5 ppm $H_2CO$ concentrations. Reproducibility was confirmed by exposing the sensor to 1.7-ppm $H_2CO$ for three consecutive cycles. The response was similar across all three cycles, with no significant changes in response, response time, or recovery time. The proposed QCM sensor's detection limit is ~ 0.06 ppm, within the WHO's proposed safe exposure limits. The functionalized QCM was further exposed to ethanol, acetone, chloroform, benzene, and toluene to determine its selectivity. The GO-QCM sensor demonstrated high selectivity and responsivity to formaldehyde.

Copper–manganese composite oxide was synthesized by Yang and He [53] for use as a sensing layer over a QCM sensor for detecting formaldehyde gas. The composite was dropcasted over a silver QCM electrode. The experiment took place in a glass chamber inside an incubator at 20 °C; here, gas containing various formaldehyde concentrations (0.3–1.7 ppm) was introduced. The prepared sensor showed a descending frequency response to the gas at a formaldehyde concentration of 1.7, reaching − 270 Hs in 60 s. The copper–manganese composite-coated QCM frequency shift and recovery (flushing the sensor with air) is shown in Fig. 16. There were no significant changes in the sensing profile after 10, 30, and 60 days; thus, the composite appears relatively stable. Different volatile chemicals were used to study the prepared sensor's selectivity. Our results indicated that ethanol might interfere with formaldehyde. The prepared sensor could monitor formaldehyde in real time due to the linearity between the QCM and formaldehyde concentrations.

Many chemicals are toxic to humans, with the potential to damage eyes, skin, and airways. Podder et al. [54] fabricated a WCPCF using Topas. This chemical sensor, consisting of a rectangular core and 12 clad holes, was fabricated to detect Tabun, Soman, and Sarin at the THz range. We used fixed hole lengths and strut variations (i.e., the space between the holes) of 20, 14, and 8 µm. The relative sensitivities to the three chemicals at 2.6 THz were 94.34% for Sarin, 95.23% for Soman, and 96.12% for Tabun. Although the smallest between-hole spacing (8 cm) had the

highest sensitivity, the researchers selected the 14-μm strut for ease-of-fabrication. Since the light is confined at high frequencies, they observed greater sensitivity for higher operating frequencies. The researchers also found the sensor's effective area to be higher for Sarin due to its lower RI. For example, light within the core spreads more when chemicals with a low refractive indices are used. Table 1 presents a comparison between the sensitivity and limit of detection for different QCM based sensors.

## 4 Conclusion and Future Prospective

General research devoted to applying the QCM technique for the development of biosensors encompasses a wide range of potential applications that include, amongst others, drug screening, diagnosis, detection of chemical and biological species, monitoring of cellular responses and immunoassays have been presented in this paper. The use of coatings and surface modifiers in the form of functionalized nanoparticles, polymers and complexes has been extensively explored. The use of QCM sensors in various biological and chemical applications has proven to be promising at delivering optimized approaches to enhance the sensitivity and selectivity of the sensors to detect biological and molecular targets. The QCM could be optimized based on the desired criteria. The selectivity of biological sensors may be tailored for specified targeted samples. This is demonstrated in several cases as ZnO nanotips functionalized with DNA, mouse hybridridoma IgM isotype antibodies, iron oxide nanoparticles, gill epithelial cells, and polymer brushes. As for QCM chemical sensors, the detection of volatile organic compounds, formaldehyde, and benzene detection has been enhanced by various coating materials such as chitosan polymer, graphene oxide, and MOFs, and by implementing the MIP technique.

Although the developed QCM system here presented inherently lacks dissipation monitoring capabilities, it demonstrated to be a promising low-cost technique for rapid detection with potential use in point-of-care applications. QCM substrates functionalization with biochemical species and inclusively the formation of graphene oxide-supported biotinylated lipid monolayers or the use of helper molecules are possibilities to be explored. One of the main open challenges is the improvement of the crystal coating technique to ensure that uniform and solid deposition layers have been formed. Finally, it is proposed to find adequate routes for increasing the reusability of QCM sensors so that the accessibility to the system could be further improved.

Another major challenge is due to the extreme frequency drift in liquid phase, QCM system for liquid application should be improved and enhanced. It needs to be more explored. Two setup platforms which were working for gas phase and liquid phase exist its own weaknesses, which need to continuously improved and enhanced, like stability and sensitivity of oscillator circuits, reducing the effect factors of temperature, viscosity and density of liquid. The oscillator circuit should be added more functional components, like filter, inductor, amplifier, and so on, to work in gas and liquid phase better.

**Table 1** Comparison of the QCM-based sensor's sensitivity and limit of detection

| Type of application | Detector layer | Target | Limit of detection | Sensitivity | Ref. |
|---|---|---|---|---|---|
| Biochemical | ZnO nanostructure | DNA oligonucleotides | 264.939 ng | 10 times more sensitive than a standard QCM sensor | [7] |
| Biological | Antibodies and iron oxide nanoparticles | Glomalin protein in soil | 2.4 µg/g | Above 1 µg/g | [47] |
| Biological | Rainbow trout gill epithelial cells | Pentachlorophenol toxicant | 0.526 µM | | [38] |
| Biosensor | Polymer brush | SARS-CoV-2 | $6.7 \times 10^3$ PFU/mL | | [39] |
| Biological | Gold nanoparticles | *Salmonella typhimurium* | | | [36] |
| Biological | NanoMIP | *N*-hexanoyl-L-homoserine lactone | 1 µM | | [30] |
| Biological | Graphene oxide-MIP | Dengue type 1 virus (DENV-1) | 0.58 PFU/mL | 2.5 | [31] |
| Biological | Nano-MIP with HSA template | HSA | 16.2 µg/mL | | [32] |
| Biological | Amorphous metal–organic cage and signal probe DNA complex | miRNA (let-7a) | 247 aM | 40 µL | [40] |
| Biological | Antiteraspanin antibodies and ICAM-1 | Exomeres and exosomes | | | [41] |
| Biological | Poly(boric acid) Hydrogel | Glucose | 3 mg/L | 3.6–36 mg/L | [33] |
| Biological | C8 SAMS and SB SAMs | BSA and FBS solutions | | | [42] |
| Biological | Dichloromethane and sealant composite | Geraniol | 100 ppm of geraniol vapor | 0.52 Hz/ppm | [34] |
| Chemical | Chitosan polymer | VOC compounds | 3.3 mg/L | Highest sensitivity for n-Amyl alcohol: 4.4 Hz/mgL<br>Lowest sensitivity for acetone: 0.1 Hz/mgL | [8] |
| Chemical | Graphene oxide | Formaldehyde (HCHO) | Ca. 0.06 ppm | Ca. 22.9 Hz/ppm | [52] |
| Chemical | MOF-14 | Benzene vapor | 150 ppm | 1200 Hz @ 80 ppm | [48] |
| Chemical | Polystyrene | Effect of UV on polystyrene thin film | | | [46] |
| Chemical | PDMS microcolumns over graphene oxide flakes | VOC compounds | 80 ng/cm$^2$ | Sensitivity at the ng level | [45] |

**Table 1** (continued)

| Type of application | Detector layer | Target | Limit of detection | Sensitivity | Ref. |
|---|---|---|---|---|---|
| Chemical | Macrocycle materials (SB77) | Aromatic BTX hydrocarbons | | 31.7 Hz/number of layers | [49] |
| Chemical | Calix Resorcinarenes | Heavy metal in an aqueous solution | For cadmium ions: 0.32 ppm | For cadmium ions: 0.225 Hz/ppm | [50] |
| | | | For ionophore I:0.18 ppm for copper and 0.2 ppm for lead | For ionophore I:0.028 Hz/ppm for copper and 0.048 Hz/ppm | |
| Chemical | Copper–manganese composite | Formaldehyde | 1.7 ppm | 6.35 Hz/μg ppm | [53] |
| Chemical | Enantiomeric macrocycles bearing chiral moieties | Lead (II) ions | For complex B: 0.45 ppm | In order of 0.008 and 0.020 Hz/ppm | [51] |
| | | | For complex C: 0.30 ppm | | |

In addition, the QCM as an e-nose is an attractive technology due to its simplicity, and sensitivity; however, it is a slightly bulky instrument. Thus, it is of great interest to develop a miniaturized QCM. We believe that this review article will be useful to the scientific communities working in this domain in planning their fabrications and experiments to address the above-mentioned challenges and future prospective.

**Author contributions** AA and NA conceptualized the idea. M.A wrote the main manuscript text. NA and AA reviewed the manuscript.

## Declarations

**Conflict of interest** The authors declare no conflict of interest.

## References


1. Virgil, B. E. (1981). *Introduction to quartz crystal unit design*. Van Nostrand.
2. Mason, W. P. (1950). *Piezoelectric crystals and their applications to ultrasonics*. Van Nostrand.
3. Curie, J., & Curie, P. (1880). Développement, par pression, de l'électricité polaire dans les cristaux hémièdres à faces inclinées. *Comptes Rendus, 91*, 294–295.
4. Gautschi, D.-I.E.G. (2002). *Piezoelectric sensors*. Springer.
5. Sauerbrey, G. (1959). Verwendung von Schwingquarzen zur Wägung dünner Schichten und zur Mikrowägung. *Zeitschrift für physik, 155*(2), 206–222.
6. Ferreira, G. N., Da-Silva, A. C., & Tomé, B. (2009). Acoustic wave biosensors: Physical models and biological applications of quartz crystal microbalance. *Trends in Biotechnology, 27*(12), 689–697.
7. Reyes, P. I., Zhang, Z., Chen, H., Duan, Z., Zhong, J., Saraf, G., & Boustany, N. N. (2009). A ZnO nanostructure-based quartz crystal microbalance device for biochemical sensing. *IEEE Sensors Journal, 9*(10), 1302–1307.
8. Triyana, K., Sembiring, A., Rianjanu, A., Hidayat, S. N., Riowirawan, R., Julian, T., & Roto, R. (2018). Chitosan-based quartz crystal microbalance for alcohol sensing. *Electronics, 7*(9), 181.
9. Buttry, D. A., & Ward, M. D. (1992). Measurement of interfacial processes at electrode surfaces with the electrochemical quartz crystal microbalance. *Chemical Reviews, 92*(6), 1355–1379.
10. Na Songkhla, S., & Nakamoto, T. (2021). Overview of quartz crystal microbalance behavior analysis and measurement. *Chemosensors, 9*(12), 350.
11. King, W. H., Jr. (1964). Piezoelectric sorption detector. *Analytical Chemistry, 36*(9), 1735–1739.
12. Alder, J. F., & McCallum, J. J. (1983). Piezoelectric crystals for mass and chemical measurements. A review. *The Analyst, 108*(1291), 1169–1189.
13. McCallum, J. J. (1989). Piezoelectric devices for mass and chemical measurements: An update. A review. *The Analyst, 114*(10), 1173–1189.
14. Kanazawa, K. K., & Gordon, J. G. (1985). The oscillation frequency of a quartz resonator in contact with liquid. *Analytica Chimica Acta, 175*, 99–105.
15. Bruckenstein, S., & Shay, M. (1985). Experimental aspects of use of the quartz crystal microbalance in solution. *Electrochimica Acta, 30*(10), 1295–1300.
16. Schmitt, N., Tessier, L., Watier, H., & Patat, F. (1997). A new method based on acousticimpedance measurements for quartz immunosensors. *Sensors and Actuators B: Chemical, 43*(1), 217–223.
17. Bizet, K., Gabrielli, C., Perrot, H., & Therasse, J. (1998). Validation of antibody-basedrecognition by piezoelectric transducers through electroacoustic admittance analysis. *Biosensors and Bioelectronics, 13*(3), 259–269.
18. Schmitt, R. F., Allen, J. W., Vetelino, J. F., Parks, J., & Zhang, C. (2001). Bulk acoustic wave modes in quartz for sensing measurand-induced mechanical and electrical property changes. *Sensors and Actuators B: Chemical, 76*(1), 95–102.
19. Kanazawa, K. K. (2002). Steady state and transient QCM solutions at the metal| solution interface. *Journal of Electroanalytical Chemistry, 524*, 103–109.

20. Welsch, W., Klein, C., Von Schickfus, M., & Hunklinger, S. (1996). Development of a surface acoustic wave immunosensor. *Analytical Chemistry, 68*(13), 2000–2004.
21. Wessa, T., Rapp, M., & Ache, H. (1999). New immobilization method for SAW-biosensors: Covalent attachment of antibodies via CNBr. *Biosensors and Bioelectronics, 14*(1), 93–98.
22. Dahint, R., Grunze, M., Josse, F., & Renken, J. (1994). Acoustic plate mode sensor for immunochemical reactions. *Analytical Chemistry, 66*(18), 2888–2892.
23. Dahint, R., Seigel, R. R., Harder, P., Grunze, M., & Josse, F. (1996). Detection of nonspecific protein adsorption at artificial surfaces by the use of acoustic plate mode sensors. *Sensors and Actuators B: Chemical, 36*(1), 497–505.
24. Kovacs, G., Vellekoop, M., Haueis, R., Lubking, G., & Venema, A. (1994). A Love wave sensor for (bio) chemical sensing in liquids. *Sensors and Actuators A: Physical, 43*(1), 38–43.
25. Harding, G., Du, J., Dencher, P., Barnett, D., & Howe, E. (1997). Love wave acoustic immunosensor operating in liquid. *Sensors and Actuators A: Physical, 61*(1), 279–286.
26. Muramatsu, H., Tamiya, E., & Karube, I. (1988). Computation of equivalent circuit parameters of quartz crystals in contact with liquids and study of liquid properties. *Analytical Chemistry, 60*(19), 2142–2146.
27. Afzal, A., Mujahid, A., Schirhagl, R., Bajwa, S. Z., Latif, U., & Feroz, S. (2017). Gravimetric viral diagnostics: QCM based biosensors for early detection of viruses. *Chemosensors, 5*(1), 7.
28. Martin, S. J., Granstaff, V. E., & Frye, G. C. (1991). Characterization of a quartz crystal microbalance with simultaneous mass and liquid loading. *Analytical Chemistry, 63*(20), 2272–2281.
29. Pohanka, M. (2018). Overview of piezoelectric biosensors, immunosensors and DNA sensors and their applications. *Materials, 11*(3), 448.
30. Guha, A., Ahmad, O. S., Guerreiro, A., Karim, K., Sandström, N., Ostanin, V. P., & Ghosh, S. K. (2020). Direct detection of small molecules using a nano-molecular imprinted polymer receptor and a quartz crystal resonator driven at a fixed frequency and amplitude. *Biosensors and Bioelectronics, 158*, 112176.
31. Navakul, K., Sangma, C., Yenchitsomanus, P. T., Chunta, S., & Lieberzeit, P. A. (2021). Enhancing sensitivity of QCM for dengue type 1 virus detection using graphene-based polymer composites. *Analytical and Bioanalytical Chemistry, 413*(24), 6191–6198.
32. Sudjarwo, W. A. A., Dobler, M. T., & Lieberzeit, P. A. (2022). QCM-based assay designs for human serum albumin. *Analytical and bioanalytical chemistry, 414*(1), 731–741.
33. Dou, Q., Zhang, Z., Wang, Y., Wang, S., Hu, D., Zhao, Z., & Dai, Q. (2020). Ultrasensitive poly (boric acid) hydrogel-coated quartz crystal microbalance sensor by using UV pressing-assisted polymerization for saliva glucose monitoring. *ACS Applied Materials & Interfaces, 12*(30), 34190–34197.
34. Roy, S., Nag, S., Banerjee, M. B., Dasgupta, S., Pramanik, P., & Bandyopadhyay, R. (2022). Detection of geraniol in Palmarosa essential oil using silicone sealant as molecularly imprinted polymer in a QCM sensor. *Journal of Materials NanoScience, 9*(2), 120–124.
35. Taratula, O., Galoppini, E., Mendelsohn, R., Reyes, P. I., Zhang, Z., Duan, Z., & Lu, Y. (2009). Stepwise functionalization of ZnO nanotips with DNA. *Langmuir, 25*(4), 2107–2113.
36. Ortega-Valencia, J. E., Oliva-Ramírez, J., García-Barradas, O., Jiménz-Fernández, M., Rosas-Saito, G. H., Oseguera-Peña, J. E., & Melo-Máximo, D. V. (2022). Development of a QCM immunosensor with functionalized gold nanoparticles for the detection of *Salmonella typhimurium*. *Materials Letters, 314*, 131885.
37. Pohanka, M., & Vlcek, V. (2020). Immunoassay of glomalin by quartz crystal microbalance biosensor containing iron oxide nanoparticles. *International Journal of Analytical Chemistry*, *2020*.
38. Lee, K. L., Ng, S., Li, F., Nordin, A. N., & Voiculescu, I. (2020). MEMS biosensor for monitoring water toxicity based on quartz crystal microbalance. *Biointerphases, 15*(2), 021006.
39. Forinová, M., Pilipenco, A., Víšová, I., Kunčák, J., Lynn, N. S., Yudin, P., & Vaisocherová-Lísalová, H. Biosensor for rapid detection of SARS-CoV-2 in real-world samples. In *2021 IEEE Sensors* (pp. 1–4). IEEE.
40. Jin, X., Zhang, Y. P., Li, D. M., Ma, D., Zheng, S. R., Wu, C. H., & Zhang, W. G. (2020). The interaction of an amorphous metal–organic cage-based solid (aMOC) with miRNA/DNA and its application on a quartz crystal microbalance (QCM) sensor. *Chemical Communications, 56*(4), 591–594.
41. Liangsupree, T., Multia, E., Forssén, P., Fornstedt, T., & Riekkola, M. L. (2022). Kinetics and interaction studies of anti-tetraspanin antibodies and ICAM-1 with extracellular vesicle subpopulations using continuous flow quartz crystal microbalance biosensor. *Biosensors and Bioelectronics, 206*, 114151.

42. Mondarte, E. A. Q., Zamarripa, E. M. M., Chang, R., Wang, F., Song, S., Tahara, H., & Hayashi, T. (2022). Interphase protein layers formed on self-assembled monolayers in crowded biological environments: analysis by surface force and quartz crystal microbalance measurements. *Langmuir, 38*, 1324–1333.
43. Hossain, M., & Podder, E. (2019). Design and investigation of PCF-based blood components sensor in terahertz regime. *Applied Physics A, 125*(12), 1–8.
44. Rianjanu, A., Fauzi, F., Triyana, K., & Wasisto, H. S. (2021). Electrospun nanofibers for quartz crystal microbalance gas sensors: A review. *ACS Applied Nano Materials, 4*(10), 9957–9975.
45. Son, J., Ji, S., Kim, S., Kim, S., Kim, S. K., Song, W., & Myung, S. (2021). GC-like graphene-coated quartz crystal microbalance sensor with microcolumns. *ACS Applied Materials & Interfaces, 13*(3), 4703–4710.
46. Alodhayb, A. N. (2022). Measurement of polystyrene photodegradation rate using a quartz crystal microbalance. *IET Nanobiotechnology, 16*(2), 61.
47. Wang, L. (2020). Metal-organic frameworks for QCM-based gas sensors: A review. *Sensors and Actuators A: Physical, 307*, 111984.
48. Ma, Z., Yuan, T., Fan, Y., Wang, L., Duan, Z., Du, W., & Xu, J. (2020). A benzene vapor sensor based on a metal-organic framework-modified quartz crystal microbalance. *Sensors and Actuators B: Chemical, 311*, 127365.
49. Zeybek, N., AÇIKBAŞ, Y., Bozkurt, S., Sirit, A., Capan, R., ERDOĞAN, M., & ÖZKAYA, C. (2021). Developing of the calixarene based diamide chemical sensor chip for detection of aromatic hydrocarbons' vapors. *Balıkesir Üniversitesi Fen Bilimleri Enstitüsü Dergisi, 23*(1), 291–300.
50. Shaban, A., & Eddaif, L. (2021). Comparative Study of a sensing platform via functionalized calix[4]resorcinarene Ionophores on QCM resonator as sensing materials for detection of heavy metal ions in aqueous environments. *Electroanalysis, 33*(2), 336–346.
51. Eddaif, L., Shaban, A., Telegdi, J., & Szendro, I. (2020). A piezogravimetric sensor platform for sensitive detection of lead (ii) ions in water based on calix[4]resorcinarene macrocycles: Synthesis, characterization and detection. *Arabian Journal of Chemistry, 13*(2), 4448–4461.
52. Yang, M., & He, J. (2016). Graphene oxide as quartz crystal microbalance sensing layers for detection of formaldehyde. *Sensors and Actuators B: Chemical, 228*, 486–490.
53. Yang, M., & He, J. (2018). A copper–manganese composite oxide as QCM sensing layers for detection of formaldehyde gas. *RSC advances, 8*(1), 22–27.
54. Podder, E., Hossain, M. B., Rahaman, M. E., Mondal, H. S., Kabiraj, S., & Raihan, M. (2021). Design and optimization of the perilous chemical sensor in the terahertz frequency range. *Materials Today: Proceedings, 43*, 3720–3724.



## Authors and Affiliations

**Nadyah Alanazi[1] · Maram Almutairi[1] · Abdullah N. Alodhayb[1,2]**

✉ Abdullah N. Alodhayb
aalodhayb@ksu.edu.sa

[1] Department of Physics and Astronomy, College of Science, King Saud University, Riyadh 11451, Saudi Arabia

[2] King Abdullah Institute for Nanotechnology, King Saud University, Riyadh 11451, Saudi Arabia